Two-dimensional steady-state thermal elasto-plastic contact of rough surfaces

G Liu[1*], **T Liu**[1,3], **Q Xie**[1], and **Q J Wang**[2]
[1]School of Mechatronic Engineering, Northwestern Polytechnical University, Xi'an, People's Republic of China
[2]Department of Mechanical Engineering, Northwestern University, Evanston, Illinois, USA
[3]Institute of Mechanics and Computational Mechanics, Leibniz University of Hannover, Hannover, Germany

The manuscript was received on 18 November 2007 and was accepted after revision for publication on 23 June 2008.

DOI: 10.1243/13506501JET400

Abstract: A finite-element deterministic two-dimensional thermal elasto-plastic contact model is presented in this article, which facilitates the investigation of the influence of steady-state frictional heating on contacting asperities and subsurface stress fields. This model takes into account the asperity distortion caused by the temperature variation in a tribological process, microplastic flow of surface asperities, and coupled thermo-elasto-plastic behaviour of the material, with and without considering the strain-hardening property of the material. The model is verified through the contact analysis of a rigid, isothermal cylinder with a thermally conductive, elasto-plastic plane. The maximum contact pressures increase with frictional heating. Furthermore, thermal effects on the contact pressure, real area of the contact, and average gap of a real rough surface with different frictional heat inputs under thermal elasto-plastic contact conditions are numerically investigated. It indicates that neglecting thermal effect overestimates the real area of the contact and underestimates the average gap between the contacting surfaces.

Keywords: steady state, thermal elasto-plastic, contact, rough surfaces

1 INTRODUCTION

One of the important issues in analysing tribological systems is the asperity contact subjected to the heat transfer across contact interfaces. Variations in temperature rise at contact interfaces induced by frictional heating may produce thermal expansion and asperity distortion, which cause the contact pressure distribution and the real area of contact to change. Many works have been carried out in developing asperity contact models under thermoelastic conditions. Early studies were mainly focused on Hertzian-contact or single asperity-contact problems for thermal stresses [**1**–**7**], which indicated that the influence of temperature on contacting surfaces due to friction should be considered in the analysis of contacting bodies. Barber [**2**] gave resolution of steady-state thermoelastic contacts between two semi-infinite solids with some simplification assumptions. Azarkin *et al.* [**3**] presented a numerical procedure that combined thermoelastic and mechanical behaviours in frictional sliding and investigated the contact pressures between contacting surfaces and stress and strain distributions in the contacting bodies of different materials. Bryant *et al.* [**4**] presented a particle ejection theory. By using this theory, thermal stress and fracture fields of wear in association with thermal mounding on high-speed sliders can be analysed. Yevtushenko [**5**] developed a procedure that could determine the temperature fields in concentrated sliding contacts. The effect of 'hot spots' on the temperature of frictional surfaces was investigated. Ciavarella *et al.* [**6**] presented a research on the thermoelastic contact of rough surfaces, in which one of the contact bodies had a sinusoidal wavy surface. Recently, Afferrante and Liavarella [**7**] presented a research on the instability of thermoelastic contacts for two sliding half-planes and suggested conditions under which instability may occur.

Corresponding author: School of Mechatronic Engineering, Northwestern Polytechincal University, No. 127, West Youyi Road, Xi'an 710072, People's Republic of China. email: npuliug@nwpu.edu.cn

Using the finite-element method (FEM) and the mathematical programming technique, Wang and Liu [**8**, **9**] developed a thermoelastic contact model. The conjugate gradient method-based [**10**] iteration procedures were combined with the discrete convolution as fast Fourier transform method [**11**]. The thermal elasto-perfectly plastic contact model by Yu *et al.* [**12**] considered the variation of the yield strength as a function of temperature. Recently, Boucly *et al.* [**13**, **14**] developed a semi-analytical thermo-elastic-plastic model to simulate the rolling/sliding contact between two smooth and two rough surfaces.

A deterministic FEM two-dimensional steady-state thermal elasto-plastic asperity contact model is presented, in which the thermal expansion and thermal stress fields are fully coupled with the elasto-plastic behaviour of the material by using the FEM, initial stiffness method, and the incremental mathematical programming technique. The model is validated by solving the thermal elasto-plastic contact between a rigid, isothermal cylinder and a thermally conductive, elasto-plastic plane. Then, the thermal elasto-plastic contact model is used to solve the contact problems between a real rough surface and a rigid plane with different frictional heat inputs.

2 HEAT TRANSFER MODEL

A thermal–mechanical asperity contact can be modelled based on the geometry shown in Fig. 1(a) as a plane–strain problem. As the measurement of a real rough surface usually depends on the resolution and the sampling range of instruments, one needs to present a reasonable representation for a stochastic infinite rough surface by using a surface with a limited sampling length. Here, it assumes that the profile of a real random rough surface may be numerically generated by symmetrical extensions of a profile digitized in a finite sampling length L. If the entire surface is subjected to the same contact and heat-transfer conditions, the heat exchange and transverse deformation across the boundaries of the profile segment may be negligible because of the geometric symmetry.

The heat transfer due to asperity contact and frictional heating can be described by the heat conduction expressed by equation (1), subjected to the boundary conditions given by equation (2a) to (c)

$$\frac{\partial}{\partial x}\left(k\frac{\partial T}{\partial x}\right)+\frac{\partial}{\partial y}\left(k\frac{\partial T}{\partial y}\right)=0,\quad (x,y)\in\Omega \tag{1}$$

$$k\frac{\partial T}{\partial n_y}=-q(x),\quad (x,y)\subset \mathrm{S}_1 \tag{2a}$$

$$k\frac{\partial T}{\partial n_x}=0,\quad (x,y)\subset \mathrm{S}_2,\ \mathrm{S}_3 \tag{2b}$$

$$T=T_0,\quad (x,y)\subset \mathrm{S}_4 \tag{2c}$$

In these equations, k is the thermal conductivity of the material, and Ω is the solid domain. The thermal boundary conditions are denoted by S_1 through S_4, where S_1 is the heat-input boundary and S_2 and S_3 are the adiabatic interfaces between adjacent asperity profiles. T is the temperature rise relative to the prescribed ambient reference temperature T_0, which may be proper for the base S_4 of the present model. The asperity contact surface is subjected to pressure, traction, and frictional heating. The effects of asperity thermal distortion on contact pressure and real area of contact were taken into account in the model.

In order to simplify the solution process, material properties are assumed to be independent of temperature variation. At a surface location x_i, frictional heat flux $q(x_i)$ is proportional to the contact pressure $p(x_i)$ over a differential area ΔA or to the surface nodal force R_i

$$q(x_i)=f\nu\cdot\beta\cdot p(x_i)=\frac{f\nu\cdot\beta}{\Delta A}\cdot R_i,\quad i=1,2,\ldots,m \tag{3}$$

where f is the frictional coefficient, ν is the sliding speed, β is the heat partition coefficient, and ΔA is the differential area over the contact pressure $p(x_i)$ located at x_i. The frictional tangential nodal force is proportional to the normal nodal force and equals fR_i. In equation (3), the product of frictional coefficient and sliding speed $f\nu$ is a factor that is proportional to the heat flux and employed to measure the amount of frictional heat input. Although the current model can handle variable heat partition coefficient, β is still supposed to be constant along the contacting surfaces for simplicity. However, it should be addressed that, in reality, β is usually not a prescribed function. As can be seen in Fig. 1, the direction of the surface tractions, which is mentioned in this study, is along the positive direction of the x-axis, which means that the slider moves from right to left over the surface of the substrate.

For mechanical boundary conditions, the left and right boundaries, S_2 and S_3, are fixed along the direction x and, boundary S_4 is fixed in both x and y directions. A series of constraint coefficients, $\{d_1\}^T$, $\{d_1\}^N$, $\{d_2\}^T$, and $\{d_2\}^N$ caused by the unit shear and normal loads, and $\{D_1^T\}$, $\{D_1^N\}$, $\{D_2^T\}$, and $\{D_2^N\}$ by the real loads for boundaries BC_1 and BC_2, are introduced to evaluate the deformation along the boundaries of the calculation domain.

An extended model that deals with the shear-traction effect on the thermoelastic stress distributions was developed by Liu and Wang [**9**]. Owing to the symmetric extension of the surface profile, the tractions on the surface should also be symmetric with respect to each boundary, as shown in Fig. 1(b). For

a pair of shear and normal loads, R_{ti} and R_{ni}, at the distance x_i right to the boundary, there should exist another pair with the same magnitude located on the other side of the boundary.

3 INCREMENTAL THEOREM AND INITIAL STIFFNESS METHOD FOR THERMAL ELASTO-PLASTIC PROBLEMS

3.1 Thermal elasto-plastic stress–strain relationship

For the thermoelastic problem described in the coordinate system shown in Fig. 1(a), the stress tensor in the plane can be expressed as

$$\boldsymbol{\sigma} = \mathbf{D}_{\mathrm{e}}(\boldsymbol{\varepsilon} - \boldsymbol{\varepsilon}_0) = \mathbf{D}_{\mathrm{e}}\boldsymbol{\varepsilon} - \mathbf{D}_e\boldsymbol{\varepsilon}_0 \tag{4}$$

where $\mathbf{D}_{\mathrm{e}}$ is the elastic matrix, $\boldsymbol{\varepsilon}$ is the strain vector, and $\boldsymbol{\varepsilon}_0$ is the free thermal strain vector. For plane stress problems, $\mathbf{D}_{\mathrm{e}}\boldsymbol{\varepsilon}_0$ can be obtained as [**8**]

$$\mathbf{D}_{\mathrm{e}}\boldsymbol{\varepsilon}_0 = \frac{E\theta T_\alpha^{\mathrm{e}}}{1-\nu}\begin{pmatrix}1\\1\\0\end{pmatrix} \tag{5}$$

where θ is the thermal expansion coefficient and T_α^{e} is the element average temperature. E and ν are the Young's modulus and Poisson's ratio, respectively. For plane strain problems, E, ν, and θ in equation (6) should be substituted by $E/(1–\nu^2)$, $\nu/(1–\nu)$, and $(1+\nu)\theta$, respectively.

The von Mises yield criterion is used to predict the plastic zone. The equivalent von Mises stress, σ_{e}, is defined as

$$\sigma_{\mathrm{e}} = \sqrt{3}\cdot(J_2')^{1/2} \tag{6}$$

where J_2' is the second deviatoric stress invariant, which can be written as

$$J_2' = \frac{1}{2}[\sigma_x'^2 + \sigma_y'^2 + \sigma_z'^2] + \tau_{xy}^2 + \tau_{yz}^2 + \tau_{zx}^2 \tag{7}$$

where $\sigma_i' = \sigma_i - \bar{\sigma}(i = x, y, z)$ and $\bar{\sigma} = 1/3(\sigma_x + \sigma_y + \sigma_z)$ is the average stress. When σ_{e} is greater than the yield strength of the material, the σ_{Y}, the material begins to yield.

Owing to yielding, the stress–strain relationship of the material is no longer linear, and an elasto-plastic stress–strain relationship has been introduced [**15**]. By including the thermal effect, the stress increments during any load increment can be obtained as follows

$$\Delta\boldsymbol{\sigma} = \mathbf{D}_{\mathrm{ep}}\cdot(\Delta\boldsymbol{\varepsilon} - \Delta\boldsymbol{\varepsilon}_0) \tag{8}$$

where $\Delta\boldsymbol{\sigma}$ is the stress increment, $\Delta\boldsymbol{\varepsilon}$ is the strain increment, $\Delta\boldsymbol{\varepsilon}_0$ is the free strain increment, and $\mathbf{D}_{\mathrm{ep}}$ is the

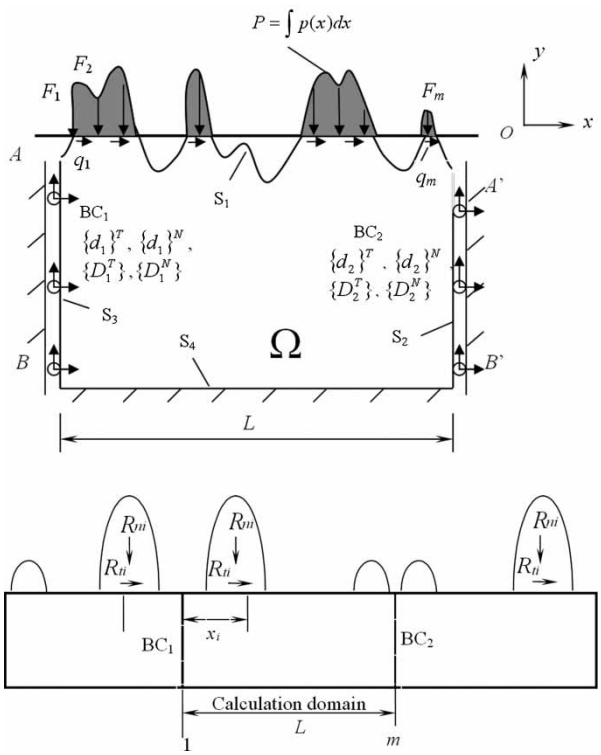

Fig. 1 Frictional heating and thermal boundary constraints defined for the thermal–mechanical asperity contact model: (a) contact, frictional heating, and thermal boundaries of a calculation domain and (b) extended domain for boundary constraint definition

elasto-plastic matrix, which can be expressed as

$$\mathbf{D}_{\mathrm{ep}} = \mathbf{D}_{\mathrm{e}} - \mathbf{D}_{\mathrm{p}} \tag{9}$$

where $\mathbf{D}_{\mathrm{e}}$ is the elastic matrix and $\mathbf{D}_{\mathrm{p}}$ is the plastic matrix, which can be expressed as

$$\mathbf{D}_{\mathrm{p}} = \mathbf{D}_{\mathrm{e}} \cdot \mathbf{q}' \cdot \mathbf{w}' \tag{10}$$

where

$$\mathbf{q}' = \frac{\sqrt{3}}{\sigma_{\mathrm{e}}} \left(\frac{\sigma_x'}{2}, \frac{\sigma_y'}{2}, \frac{\sigma_z'}{2}, \tau_{xy}, \tau_{yz}, \tau_{zx} \right)^{\mathrm{T}} \tag{11}$$

$$\mathbf{w}' = \frac{\mathbf{q}'^{\mathrm{T}} \mathbf{D}_{\mathrm{e}}}{H' + \mathbf{q}'^{\mathrm{T}} \mathbf{D}_{\mathrm{e}} \mathbf{q}'} \tag{12}$$

In equation (13), H' is the strain-hardening function related to the elasto-plastic tangential modulus, E_{T}, and can be expressed as

$$H' = \frac{E_{\mathrm{T}}}{1 - E_{\mathrm{T}}/E} \tag{13}$$

In this article, the strain-hardening property of the material is considered to be linear and isotropic. The equations mentioned earlier are also valid for elastic-perfectly-plastic materials, for which E_{T} should be zero, with H' being zero.

3.2 Initial stiffness method for thermal elasto-plastic problems

For any load increment, $\Delta\mathbf{R}^{\mathrm{m}}$, a discretized non-linear system can generally be expressed as a set of algebraic equations of the form

$$\mathbf{K}_{\mathrm{ep}} \cdot \Delta\boldsymbol{u} = \Delta\boldsymbol{R}^{\mathrm{m}} - \Delta\boldsymbol{R}^{\mathrm{t}} \tag{14}$$

where $\Delta\boldsymbol{u}$ is the displacement increment and $\Delta\boldsymbol{R}^{\mathrm{t}} = \mathbf{H} \cdot \Delta\boldsymbol{R}^{\mathrm{m}}$ is the equivalent thermal load increment, where $\mathbf{H}$ is a function that relates the equivalent thermal and the surface nodal forces. The mathematical expression of $\mathbf{H}$ for FEM programming may be found in reference [**8**]. $\mathbf{K}_{\mathrm{ep}}$ is the elasto-plastic stiffness matrix defined as

$$\mathbf{K}_{\mathrm{ep}} = \mathbf{K}_{\mathrm{e}} - \mathbf{K}_{\mathrm{p}} \tag{15}$$

where $\mathbf{K}_{\mathrm{e}}$ is the elastic stiffness matrix, which can be written as

$$\mathbf{K}_{\mathrm{e}} = \int_{\Omega} \mathbf{B}^{\mathrm{T}} \mathbf{D}_{\mathrm{e}} \mathbf{B} \, \mathrm{d}\Omega \tag{16}$$

where $\mathbf{B}$ is the strain matrix. In equation (15), $\mathbf{K}_{\mathrm{p}}$ is called the plastic stiffness matrix.

Substituting equation (15) into equation (14) results in

$$\mathbf{K}_{\mathrm{e}} \cdot \Delta\boldsymbol{u} = \Delta\boldsymbol{R}^{\mathrm{m}} - \Delta\boldsymbol{R}^{\mathrm{t}} + \Delta\boldsymbol{R}_{\sigma} \tag{17}$$

where $\Delta\boldsymbol{R}_{\sigma} = \mathbf{K}_{\mathrm{p}} \cdot \Delta\boldsymbol{u}$ is the initial force vector [**16**] or the unbalanced force vector [**17**], which is express as

$$\Delta\boldsymbol{R}_{\sigma} = -\sum \int_{\Omega} \mathbf{B}^{\mathrm{T}} \cdot \Delta\boldsymbol{\sigma}_0 \, \mathrm{d}\Omega \tag{18}$$

For each yielded element i, the incremental initial stresses $\Delta\boldsymbol{\sigma}_0^i$ are

$$\Delta\boldsymbol{\sigma}_0^i = -\mathbf{D}_{\mathrm{p}} \cdot (\Delta\boldsymbol{\varepsilon}^i - \Delta\boldsymbol{\varepsilon}_0^i) \tag{19}$$

where $\Delta\boldsymbol{\varepsilon}^i$ and $\Delta\boldsymbol{\varepsilon}_0^i$ are the incremental strain vector and free thermal strain vector of the yielded element i, respectively. The corresponding elemental initial force is given as

$$\Delta\boldsymbol{R}_{\sigma}^i = -\int_{\Omega} \mathbf{B}^{\mathrm{T}} \cdot \Delta\boldsymbol{\sigma}_0^i \, \mathrm{d}\Omega \tag{20}$$

The total initial force of equation (18) can be written as the sum of the yielded elemental initial force vectors as

$$\Delta\boldsymbol{R}_{\sigma} = \sum \Delta\boldsymbol{R}_{\sigma}^i \tag{21}$$

3.3 Iteration formulas of the thermal elasto-plastic contact problems

Combining the linear programming technique with the initial stiffness method, an incremental iteration algorithm for the elasto-plastic contact problems was presented by Liu *et al.* [**15**]. The algorithm is modified here to take thermal effects into account. By multiplying the inverse matrix of the elastic stiffness matrix, $\mathbf{K}_{\mathrm{e}}^{-1}$, to both sides of equation (17), the increment of the thermal elasto-plastic deformation can be expressed as

$$\Delta\boldsymbol{u} = \mathbf{K}_{\mathrm{e}}^{-1} \cdot \Delta\boldsymbol{R}^{\mathrm{m}} - \mathbf{K}_{\mathrm{e}}^{-1} \cdot \Delta\boldsymbol{R}^{\mathrm{t}} + \mathbf{K}_{\mathrm{e}}^{-1} \cdot \Delta\boldsymbol{R}_{\sigma} = \Delta\boldsymbol{u}_{\mathrm{e}}^{\mathrm{m}} - \Delta\boldsymbol{u}_{\mathrm{e}}^{\mathrm{t}} + \Delta\boldsymbol{u}_{\mathrm{I}} \tag{22}$$

where $\Delta\boldsymbol{u}_{\mathrm{I}}$, $\Delta\boldsymbol{u}_{\mathrm{e}}^{\mathrm{m}}$, and $\Delta\boldsymbol{u}_{\mathrm{e}}^{\mathrm{t}}$ are the plastic, elastic mechanical, and thermal deformations, respectively, which can be calculated as follows

$$\Delta\boldsymbol{u}_{\mathrm{I}} = \mathbf{K}_{\mathrm{e}}^{-1} \Delta\boldsymbol{R}_{\sigma} = \mathbf{K}_{\mathrm{e}}^{-1} \cdot \sum \int_{\Omega} -\mathbf{B}^{\mathrm{T}} \cdot \Delta\boldsymbol{\sigma}_0 \, \mathrm{d}\Omega \tag{23}$$

$$\Delta\boldsymbol{u}_{\mathrm{e}}^{\mathrm{m}} = \mathbf{K}_{\mathrm{e}}^{-1} \cdot \Delta\boldsymbol{R}^{\mathrm{m}} = \mathbf{A}^{\mathrm{m}} \cdot \Delta\boldsymbol{R}^{\mathrm{m}} \tag{24}$$

$$\Delta\boldsymbol{u}_{\mathrm{e}}^{\mathrm{t}} = \mathbf{K}_{\mathrm{e}}^{-1} \cdot \Delta\boldsymbol{R}^{\mathrm{t}} = \mathbf{K}_{\mathrm{e}}^{-1} \cdot \mathbf{H} \cdot \Delta\boldsymbol{R}^{\mathrm{m}} = \mathbf{A}^{\mathrm{t}} \cdot \Delta\boldsymbol{R}^{\mathrm{m}} \tag{25}$$

In equations (24) and (25), $\mathbf{A}^{\mathrm{m}}$ is the mechanical influence function matrix, and $\mathbf{A}^{\mathrm{t}}$ is the thermal influence

function matrix, which was explained in detail in reference [**8**].

Figure 2 illustrates the thermal–mechanical deformation of asperity contacts. The incremental iteration formulas for the jth step of loading ΔP_j can be expressed in a simplex-type form as

$$\begin{cases} -(\Delta \boldsymbol{u}_{\mathrm{ej}}^{\mathrm{m}} - \Delta \mathbf{u}_{\mathrm{ej}}^{\mathrm{t}}) + \Delta\alpha_j \cdot \boldsymbol{e} + \mathbf{I} \cdot \boldsymbol{y}_j = \mathbf{y}_{j-1} + \Delta \boldsymbol{u}_{\mathrm{Ij}} \\ \boldsymbol{e}^{\mathrm{T}} \Delta \mathbf{R}_{\mathrm{j}}^{\mathrm{m}} = \Delta P_j \end{cases} \tag{26}$$

where $\Delta\alpha_j$ is the rigid-body displacement increment, $\boldsymbol{y}_j$ is the surface separation vector after deformation or the slack vector for the jth step of loading, $\Delta \boldsymbol{R}_j^{\mathrm{m}}$ is the nodal contact force vector of the jth incremental loading, $\boldsymbol{y}_{j-1}$ is the surface separation vector at the end of the $(j-1)$th incremental loading, $\boldsymbol{e}$ is the unit vector, and $\mathbf{I}$ is the identity matrix. The von Mises yield criterion is used to determine the coupled stress level at which plastic deformation begins. The incremental iteration formulas of equation (26) is subjected to the following contact conditions

$$\begin{cases} \text{if } (y_j)_i = 0, (\Delta \boldsymbol{R}_j^{\mathrm{m}})_i \geqslant 0, & \text{within the contact area} \\ \text{if } (y_j)_i > 0, (\Delta \boldsymbol{R}_j^{\mathrm{m}})_i = 0, & \text{outside of the contact area} \end{cases} \quad (i = 1, 2, \ldots, N) \tag{27}$$

and non-negative constraints

$$(\Delta \boldsymbol{R}_j^{\mathrm{m}})_i \geqslant 0, \quad \Delta\alpha_j \geqslant 0, \quad (\Delta y_j)_i \geqslant 0, \quad (i = 1, 2, \ldots, N) \tag{28}$$

where N is the number of nodes in the possible region of the surface in contact.

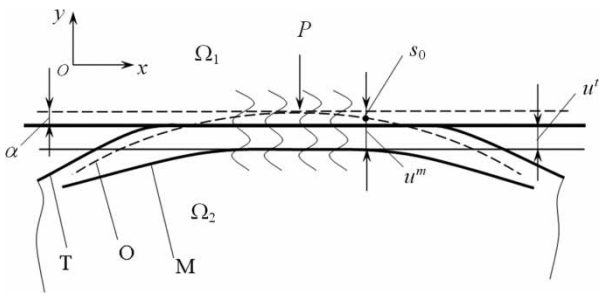

Fig. 2 Thermal deformations (O, original profile; M, deformed due to pressure; T, further deformed due to frictional heating)

3.4 Numerical implementation

The procedure for numerical implementation of the incremental-initial stiffness method for thermal elasto-plastic contact problems is given as follows.

1. Discretize the contacting bodies and form the influence matrix, $\mathbf{A}^{\mathrm{m}}$ and $\mathbf{A}^{\mathrm{t}}$, for the candidate contact nodes with the finite-element technique.
2. Calculate the contact problems under total applied load. Compute the thermo-elastic deformation $\boldsymbol{u}$, the elastic strain $\boldsymbol{\varepsilon}$, and the elastic stress $\boldsymbol{\sigma}$ and then obtain the equivalent von Mises stress, $\sigma_{\nu\mathrm{m}}$, of each element.
3. If the von Mises stress of the element $\sigma_{\nu\mathrm{m}}$ is less than the yield strength σ_{Y}, go to step 4, else go to step 6.
4. Begin to increase the applied load and set the load increment counter $j = 1$.
   (a) Compute the load increment ΔP_j.
   (b) Set iteration counter IE $= 1$ and $\Delta \boldsymbol{u}_{\mathrm{Ij}} = 0$ for the first iteration.
   (c) Calculate the surface separation vector $\boldsymbol{y}_{0j} = \boldsymbol{y}_{j-1} + \Delta \boldsymbol{u}_{\mathrm{Ij}}$. For the first load increment, $\boldsymbol{y}_{01} = \boldsymbol{y}_0$ is the initial separation.
   (d) Evaluate the nodal load increment $\Delta \boldsymbol{R}_j^{\mathrm{m}}$ and the deformed separation $\boldsymbol{y}_j$.
   (e) Calculate the increment equivalent thermal nodal forces $\Delta \boldsymbol{R}_j^{\mathrm{t}}$ under $\Delta \boldsymbol{R}_j^{\mathrm{m}}$ and the temperature rise increment $\Delta \boldsymbol{T}_j$.
   (f) Compute the increments of the elastic deformation $\Delta \boldsymbol{u}_{\mathrm{e}j}^{\mathrm{m}} = \mathbf{K}_{\mathrm{e}}^{-1} \cdot \Delta \boldsymbol{R}_j^{\mathrm{m}}$, and the thermal deformation $\Delta \boldsymbol{u}_{\mathrm{e}j}^{\mathrm{t}} = \mathbf{K}_{\mathrm{e}}^{-1} \cdot \Delta \boldsymbol{R}_j^{\mathrm{t}}$.
   (g) Calculate the thermo-elastic strain and stress increments by using the total deformation increments $\Delta \boldsymbol{u}_{\mathrm{e}j} = \Delta \boldsymbol{u}_{\mathrm{e}j}^{\mathrm{m}} - \Delta \boldsymbol{u}_{\mathrm{e}j}^{\mathrm{t}}$.
   (h) Accumulate the total strains and stresses and monitor the equivalent von Mises stress of each element to check whether the element yields according to the von Mises yield criterion.
   (i) For the yield element, compute the modified plastic deformation increments $\Delta \boldsymbol{u}_{\mathrm{Ij}}$.
   (j) Check if $\Delta \boldsymbol{u}_{\mathrm{Ij}}$ convergence (accuracy controlled as $\max\{\Delta \boldsymbol{u}_{\mathrm{Ij}} / \boldsymbol{u}_{\mathrm{Ij}}\} \leqslant 0.01$ per cent)? If yes, go to step 5, else set IE $=$ IE $+ 1$ and go to step 4(c).
5. If j equals to the total increment number, go to step 6, otherwise set $j = j + 1$ and go to step 4(a).
6. Output the results. End.

4 THERMAL ELASTO-PLASTIC CONTACT BETWEEN CYLINDER AND PLANE

The thermal elasto-plastic contact between a rigid, isolated cylinder and a conductive, elasto-plastic plane is studied to verify the present model. The radius of the cylinder is 0.5 mm, the Young's modulus and Poisson's ratio are $E = 200$ GPa and $\nu = 0.3$, and two elasto-plastic tangential moduli are $E_{\mathrm{T}} = 0$ and $E_{\mathrm{T}} = 0.1E$.

The thermal conductivity is $k = 50.2\,\mathrm{W/m\,K}$, the thermal expansion coefficient is $\theta = 11.7\,\mu\mathrm{m/m\,K}$, and the heat partition coefficient is $\beta = 1$. The length of the calculation domain L is 0.128 mm. The normal load is 15 N/mm and the yield strength of the plane is $\sigma_Y = 600\,\mathrm{MPa}$. The elasto-plastic plane is discretized into 22 832 three-node triangular finite elements and 11 603 nodes. The number of possible contact nodes on the contacting surfaces is 257. On the surface, there are 40 layers of fine elements with the vertical nodal space of 0.9625 μm, and the other elements are coarse with different vertical nodal spaces.

As the basis of the present model, Wang and Liu [**8**] compared the numerical results of the thermoelastic contacts of sinusoidal multi-asperities having different values of fv with the theoretical results presented by Johnson [**18**]. They suggested that for a value of fv lower than 0.5, the contact pressure distributions were close to Johnson's theoretical results. The calculation domain of the present model is taken as the same as that of the thermoelastic model presented by Wang and Liu's [**8**] study, in which the depth of the domain is about 0.8 times of the length L.

The relationships between the non-dimensional contact pressure p/P_0 and the non-dimensional contact half width x/a for different frictional heat inputs and frictional coefficients are given in Figs 3(a) to (c), where $fv = 0.0$ is the solution without considering the thermal effect and P_0 and a are the maximum

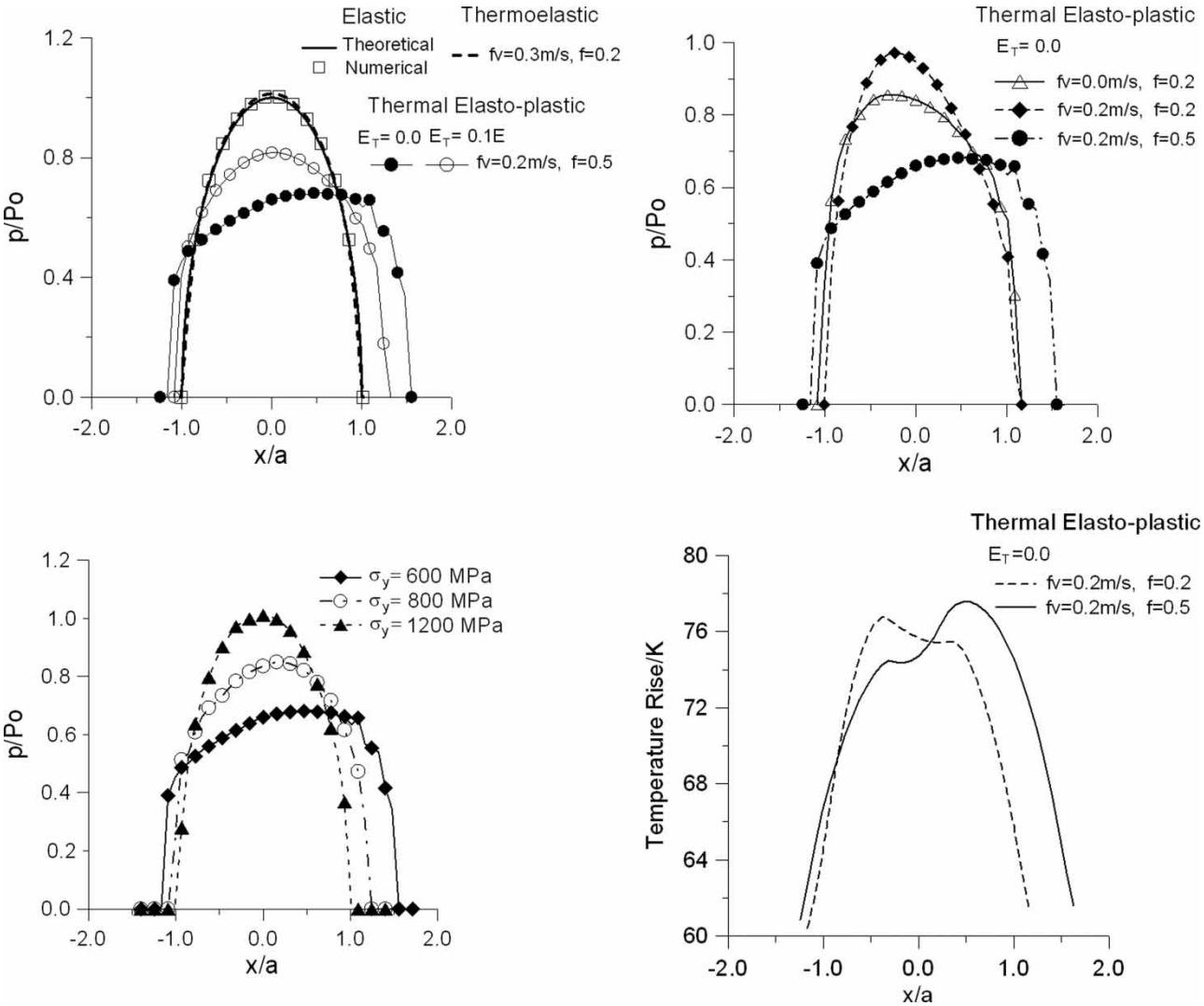

Fig. 3 Pressure distributions and temperature rise of the elastic and thermal elasto-plastic contacts with different frictional heat inputs and frictional coefficients: (a) pressures with yield strength $\sigma_\mathrm{Y} = 600\,\mathrm{MPa}$; (b) pressures when when $E_\mathrm{T} = 0.0$ with yield strength $\sigma_\mathrm{Y} = 600\,\mathrm{MPa}$; (c) pressures considering the effect of frictional shear subject to different yield strengths when $fv = 0.2\mathrm{m/s}$, $f = 0.5$; and (d) temperature rise distributions on the contacting surface when $E_\mathrm{T} = 0.0$ with yield strength $\sigma_\mathrm{Y} = 600\,\mathrm{MPa}$

contact pressure and the contact half width of the theoretical Hertzian solution, respectively. Six different cases – elastic, elastic-perfectly-plastic, elasto-plastic, thermoelastic, thermal elastic-perfectly-plastic, and thermal elasto-plastic – are shown in Figs 3(a) and (b). In Fig. 3(a), the results of the elastic contact agree well with the Hertzian solution. The maximum contact pressure of the thermoelastic contact of $fv = 0.3$ m/s is $1.0136P_0$, which is higher than that of the Hertzian contact because of thermal expansion. It can be observed that the influence of frictional shear is small for thermoelastic cases but significant for thermal elasto-plastic cases. In Fig. 3(b), for thermal elasto-plastic contacts with the same frictional coefficient, the maximum contact pressures increase, but the real areas of contact decrease with the frictional heat input. It also reveals that the contact pressures are no longer symmetric, but skew when the fictional coefficient is not zero. Figure 3(c) compares the contact pressures with different yield strengths for $fv = 0.2$ m/s and $f = 0.5$ with $E_T = 0$. Three yield strengths are chosen: $\sigma_Y = 600$ MPa, $\sigma_Y = 800$ MPa, and $\sigma_Y = 1200$ MPa. When the yield strength increases, the degree of asymmetry of the contact pressure decreases. When the yield strength is 1200 MPa, the contact pressures are still elastic and symmetrical, because the contact stresses do not exceed the yield strength under the normal load $P = 15$ N/mm. The comparison proves that plastic deformation of contacting bodies results in contact pressure asymmetry. In Fig. 3(d), the temperature rise distributions on the elasto-plastic surface with different parameters are presented. When $fv = 0.0$, as there is no thermal effect, the temperature rise is equal to zero at every contact point. When the frictional shear is taken into account, it can be seen from Fig. 3(d) that the temperature rises are no longer symmetric with the centre-line of the contact region and move with the surface tractions.

As shown in Fig. 4, the subsurface von Mises stress contours of the thermoelastic and thermal elasto-plastic contact with and without strain hardening ($E_T = 0.0$ and $E_T = 0.1E$, respectively) are presented, under the condition of different values of $fv = 0.0$, 0.1, 0.2, and 0.5 m/s and $f = 0.2$. The yield strength is $\sigma_Y = 600$ MPa. The contours show that the plastic region of the plane tends to be reduced when the frictional heat input increases. Owing to the temperature rise of the contacting bodies, the regions with stress < 100 MPa become larger. Table 1 gives the maximum von Mises stresses of the subsurface with different frictional heat inputs. For the thermal elasto-plastic contact without strain hardening ($E_T = 0.0$), the maximum von Mises stresses almost equal the yield strength $\sigma_Y = 600$ MPa. For the thermal elastic and thermal elasto-plastic contacts with strain hardening ($E_T = 0.1E$), the maximum von Mises stress first

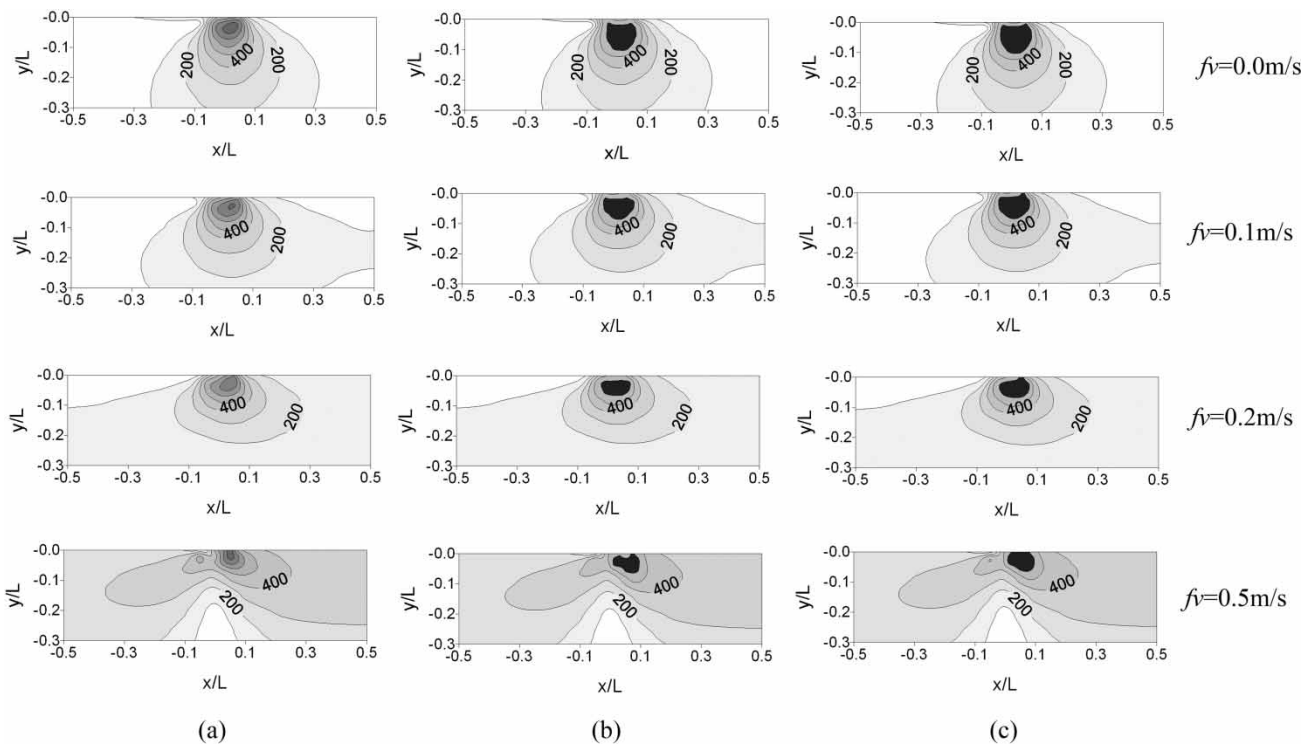

Fig. 4 Subsurface von Mises stress contours of the thermal contact under different frictional heat inputs when $f = 0.2$ (unit: MPa): (a) thermoelastic; (b) thermal elastic-perfectly-plastic, (c) thermal elasto-plastic

Table 1 Maximum subsurface von Mises stress under the thermal elastic and thermal elasto-plastic conditions with different frictional heat inputs when $f = 0.2$

Frictional heat input, fv (m/s)	Thermal elasto σ_{vm} (MPa)	Thermal elastic-plastic σ_{vm} (MPa)	
		$E_T = 0.0$	$E_T = 0.1E$
0.0	844.91	599.65	644.62
0.1	797.24	599.45	636.22
0.2	771.96	598.88	639.85
0.5	856.96	598.86	663.43

reduces and then increases with an increase of in frictional heat input. Thermal expansion plays a major role in the deformation of the contacting bodies when the frictional heat input is low. When the frictional heat input further increases, thermal expansion cannot resist the compression of mechanical deformation and the maximum von Mises stress increases. This is because that the thermal expansion and the surface compression are in the opposite direction and the variation of the stresses in the contacting bodies depends on the direction of motion during the contact process. When the parameter fv is larger, the contacting bodies are sufficiently expanded due to thermal deformation and then there is no further possibility to decrease the von Mises stress.

Figure 5 shows the comparison of the thermoelastic and thermal elasto-plastic ($E_T = 0.0$ and $E_T = 0.1E$, respectively) von Mises stresses along the depth of different locations with two values of frictional heat input, $fv = 0.0$ m/s and $fv = 0.5$ m/s, when $f = 0.5$. In Fig. 5, r is the distance from the centre-line of the contact region to the location of interest and a_c is the contact half width. Negative value of r/a_c means that the location is on the left side of the centre-line of the contact region. Figure 5 shows that the von Mises stresses of the elastic contact ($fv = 0.0$ m/s, $f = 0.5$) agree well with the theoretical solutions presented by Sackfield and Hills [**19**]. The maximum von Mises stresses of the elasto-plastic and the thermal elasto-plastic contact without strain hardening ($E_T = 0.0$) are almost equal to the yield strength of 600 MPa ($\sim 0.404P_0$), indicating that the region comes into yield under the coupled efforts of thermal and elasto-plastic stresses. As shown in Table 2, at the location of $r/a_c = -0.5$, the non-dimensional maximum von Mises stresses (σ_{vm}/P_0) of the thermoelastic and the strain-hardening thermal elasto-plastic contacts decrease with an increase in the frictional heat input because of thermal expansion. However, at the locations of $r/a_c = 0.0$ and $r/a_c = 0.5$, the non-dimensional maximum von Mises stresses subject to thermoelasticity and thermal elasto-plasticity

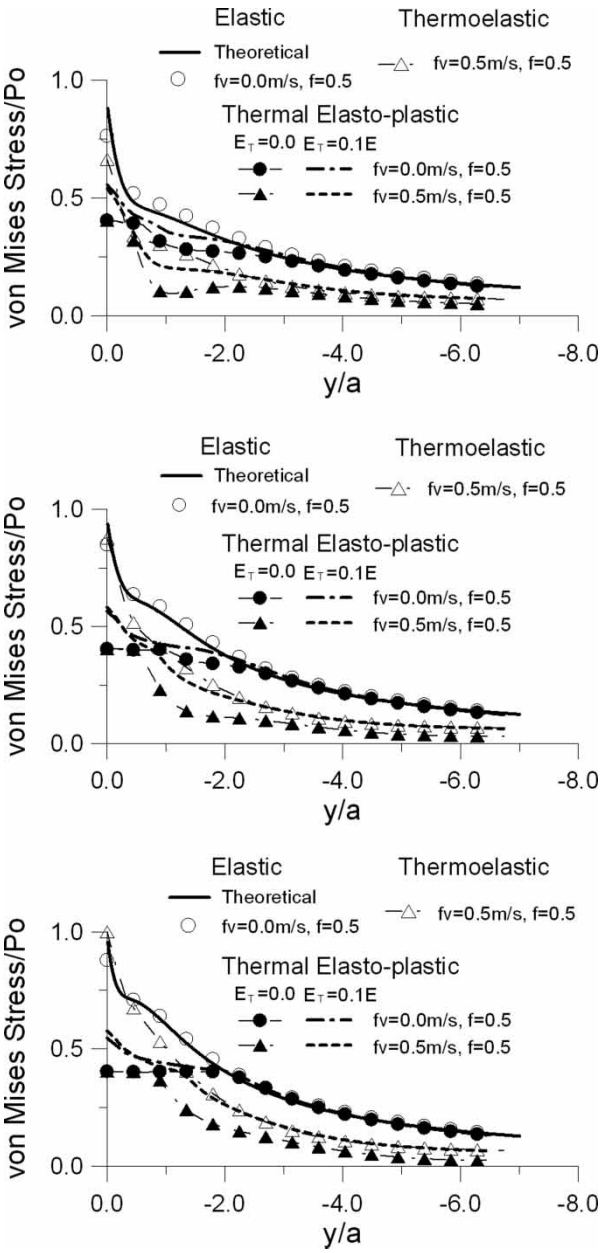

Fig. 5 Comparison of the thermoelastic and the thermal elasto-plastic von Mises stresses along the depth direction under different locations, obtained with different frictional heat inputs when $f = 0.5$: (a) $r/a_c = -0.5$, (b) $r/a_c = 0.0$, and (c) $r/a_c = 0.5$

with strain hardening are larger than the corresponding solutions without considering the thermal effect, because the thermal expansion cannot resist the compression of the contact pressure at these locations. Considering that the thermal expansion and the surface compression are in the opposite direction, the moving direction during the contact process will be a major factor influencing the change of stresses in contacting bodies.

Table 2 Non-dimensional maximum von Mises stress (σ_{vm}/P_0) obtained from the numerical calculations along the depth of different locations under the thermal elastic and thermal elasto-plastic conditions with different frictional heat inputs when $f = 0.5$

		Non-dimensional maximum von Mises stress, σ_{vm}/P_0, at different locations		
Frictional heat input, fv (m/s)		$r/a_c = -0.5$	$r/a_c = 0.0$	$r/a_c = 0.5$
Elastic/thermal elastic	$fv = 0.0$	0.76	0.85	0.88
	$fv = 0.5$	0.66	0.88	1.00
Thermal elasto- plastic ($E_T = 0.1E$)	$fv = 0.0$	0.56	0.57	0.55
	$fv = 0.5$	0.54	0.58	0.58

The subsurface von Mises stress contours of the thermoelastic and thermal elasto-plastic contacts with and without strain hardening ($E_T = 0.0$ and $E_T = 0.1E$, respectively), under different frictional heat inputs with frictional coefficient $f = 0.5$, are presented in Fig. 6. The location of the maximum Mises stress shifts towards the surface as the fictional heat input increases. Table 3 gives the maximum von Mises stress of the subsurface with different frictional heat inputs of the thermal elastic and thermal elasto-plastic contacts. Different from the cases when the frictional coefficient is $f = 0.2$, the maximum von Mises stresses of the thermal elastic and thermal elasto-plastic contacts with strain hardening increase with the frictional heat input, which again means that thermal expansion can no longer resist mechanical compression even for the lower frictional heat input when the frictional coefficient is sufficiently high.

5 THERMAL ELASTO-PLASTIC CONTACT OF ROUGH SURFACES

A thermal elasto-plastic contact problem between a flat, rigid plane and a conductive, elasto-plastic rough surface is studied in this section. The contact model is presented in Fig. 1(a). The root-mean-square (RMS) roughness is rms = 0.16 μm. The length of the rough surface is $L = 0.256$ mm. Because the RMS roughness of the surface profile used in this research is the order

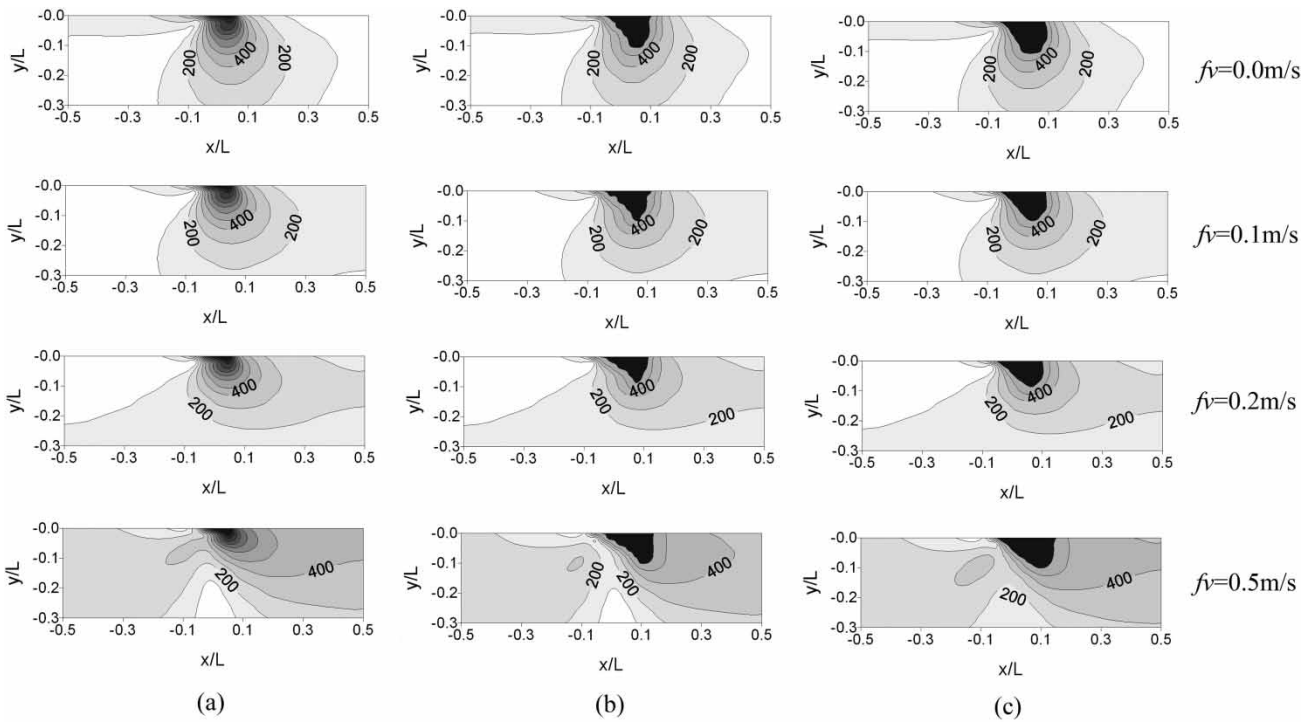

Fig. 6 Subsurface von Mises stress contours of the thermal contact under different frictional heat inputs when $f = 0.5$ (unit: MPa): (a) thermoelastic, (b) thermal elastic-perfectly-plastic, and (c) thermal elasto-plastic

Table 3 Maximum subsurface von Mises stress under the thermal elastic and thermal elasto-plastic conditions with different frictional heat inputs when $f = 0.5$

Frictional heat input, fv (m/s)	Thermal elasto σ_{vm} (MPa)	Thermal elastic-plastic, σ_{vm} (MPa)	
		$E_T = 0.0$	$E_T = 0.1E$
0.0	1166.57	599.98	841.70
0.1	1200.18	599.98	853.29
0.2	1237.45	599.98	858.79
0.5	1381.55	599.98	871.11

of 0.1–0.2 μm, 40 layers of fine elements with a vertical nodal space of 0.4 μm are meshed. The elasto-plastic plane is discretized into 22 832 three-node triangular finite elements and 11 603 nodes. The number of possible contact nodes on the contacting surfaces is 257. The geometric and material parameters are the same as those used in section 4. Two cases, $E_T = 0.0$ and $E_T = 0.1E$, are studied. The nominal pressure is, which is the equivalent uniform pressure whose sum is equal to the sum of the real pressure distribution, $p =$ 351.56 MPa. The time consumption of the calculations for the contact problems by using the FEM is one of the major effects, which should be considered. In the current model, the procedures were coded by the FORTRAN language, and the computing time is ∼1–3 h depending on different parameters, which is implemented by a computer with 1.6 GHz process speed and 512 M memory.

The non-dimensional contact pressures and the non-dimensional deformed profiles due to different frictional heat inputs and frictional coefficients, when $E_T = 0.0$ and $E_T = 0.1E$, respectively, are shown in Figs 7 and 8, where Cyd means the yield strength, σ_Y. Because the effect of strain hardening has been

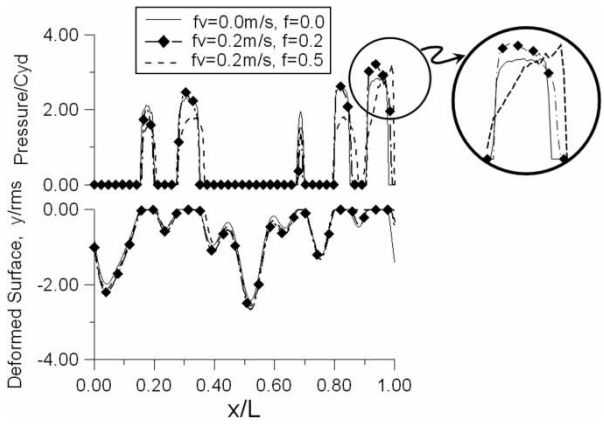

Fig. 7 Contact pressures and the deformed profiles when the rough surface is in contact with a rigid plane, $E_T = 0.0$

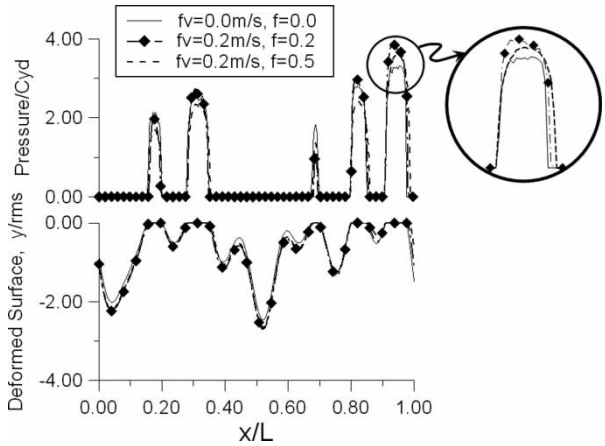

Fig. 8 Contact pressures and the deformed profiles when the rough surface is in contact with a rigid plane, $E_T = 0.1E$

included when $E_T = 0.1E$, the maximum contact pressures are larger than those for the corresponding cases when $E_T = 0.0$. It is observed that the maximum contact pressures and gaps become larger due to thermal expansion. When the frictional heat input increases, the maximum contact pressures of the contact regions associated with larger contact areas increase and those with smaller contact areas decrease. That is to say, as a result of frictional heating increases, the contacts are more and more concentrated at larger contact spots.

The subsurface von Mises stress contours of the thermal elasto-plastic contact with different frictional heat inputs, when $E_T = 0.0$ and $E_T = 0.1E$, respectively, in Figs 9 and 10, show that the plastic regions under the largest contact pressures in Figs 7 and 8 become larger with an increase in the frictional heat input, whereas the stress values of the other contact regions decrease. Table 4 gives the maximum subsurface von Mises stresses of the thermal elasto-plastic contact with different conditions when $E_T = 0.1E$. For the same frictional coefficient, the maximum von Mises stress increases with the frictional heat input.

Figure 11 gives the relationship between the non-dimensional contact pressure $\bar{p} = p^T/3\sigma_Y$ and the non-dimensional contact area $\bar{A} = A/A_{nom}$, under different frictional heat inputs and frictional coefficients, where p^T is the sum of the pressures of each contact pair on the surface, A the real area of contact and A_{nom} the nominal area of contact. Figure 12 shows the relationship between the non-dimensional average gap $\bar{h} = h_T/\text{rms}$ and the non-dimensional contact pressure $\bar{p} = p^T/3\sigma_Y$ under different frictional heat inputs and friction coefficients. The elasto-plastic tangential modulus is $E_T = 0.1E$. These two figures show that for the same frictional coefficient, the real area of contact decreases and the average gap increases

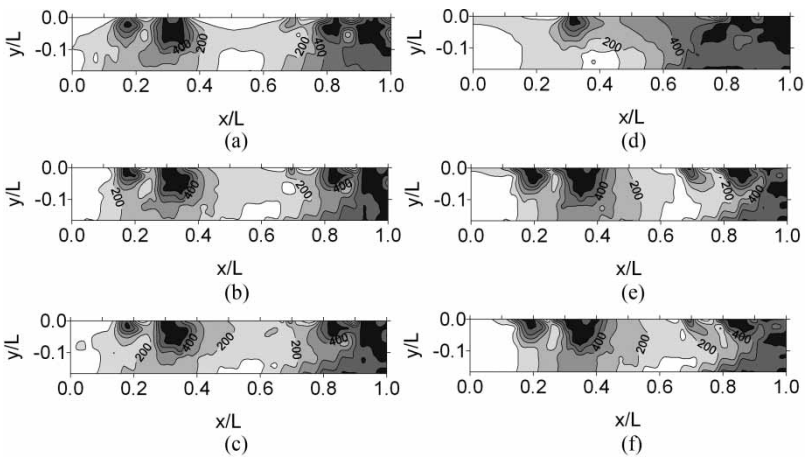

Fig. 9 Subsurface von Mises stress contours of the thermal elasto-plastic contact of the rough surface subject to different frictional heat inputs, $E_T = 0.0$ (unit: MPa): (a) $fv = 0.0$m/s, $f = 0.0$; (b) $fv = 0.1$m/s, $f = 0.2$; (c) $fv = 0.2$m/s, $f = 0.2$; (d) $fv = 0.5$m/s, $f = 0.2$; (e) $fv = 0.1$m/s, $f = 0.5$; and (f) $fv = 0.2$m/s, $f = 0.5$

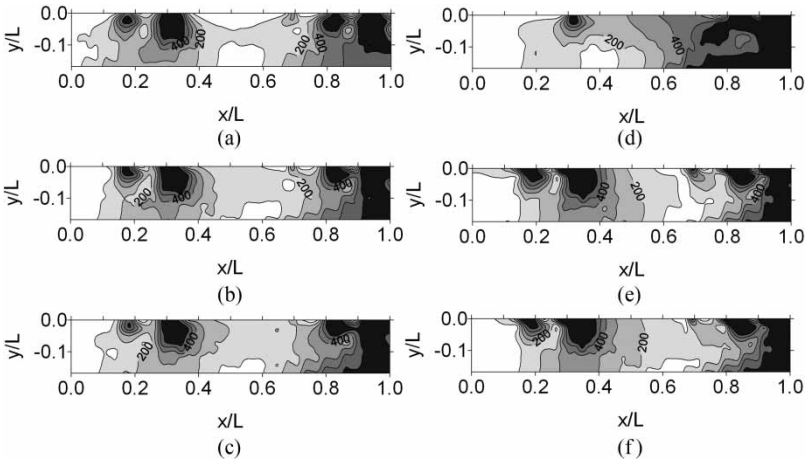

Fig. 10 Subsurface von Mises stress contours of the thermal elasto-plastic contact of the rough surface subject to different frictional heat inputs, $E_T = 0.1E$ (unit: MPa): (a) $fv = 0.0$m/s, $f = 0.0$; (b) $fv = 0.1$m/s, $f = 0.2$; (c) $fv = 0.2$m/s, $f = 0.2$; (d) $fv = 0.5$m/s, $f = 0.2$; (e) $fv = 0.1$m/s, $f = 0.5$; and (f) $fv = 0.2$m/s, $f = 0.5$

with the frictional heat input under the same contact pressure, which means that thermal expansion produces opposite displacements versus the action of the contact pressures. With the same value of frictional heat input, fv, the real area of contact becomes larger and the average gap becomes smaller with an increase in the frictional coefficient. When the contact is deeper and the value of frictional heat input, fv, is larger, the thermal effect becomes more significant. Figure 11 shows that when $fv = 0.5$ m/s, $f = 0.2$, and $\bar{p}$ is larger than 0.1, the real area of contact is significantly smaller than that due to smaller frictional heat input under the same contact pressure. In contrast, Fig. 12 shows that when $fv = 0.5$ m/s, $f = 0.2$, and $\bar{h}$ is smaller than 2.0, the average gap becomes larger when compared with that under smaller fv but the same contact pressure. These results indicate that elasto-plastic models

Table 4 Maximum subsurface von Mises stress of the thermal elasto-plastic contact between a rough surface and a rigid plane when $E_T = 0.1E$

Frictional heat input, fv (m/s)	Thermal elasto-plastic, σ_{vm} (MPa)	
	$f = 0.0$	
0.0	850.26	
	$f = 0.2$	$f = 0.5$
0.1	870.85	1628.86
0.2	880.70	1726.47
0.5	1064.62	2257.42

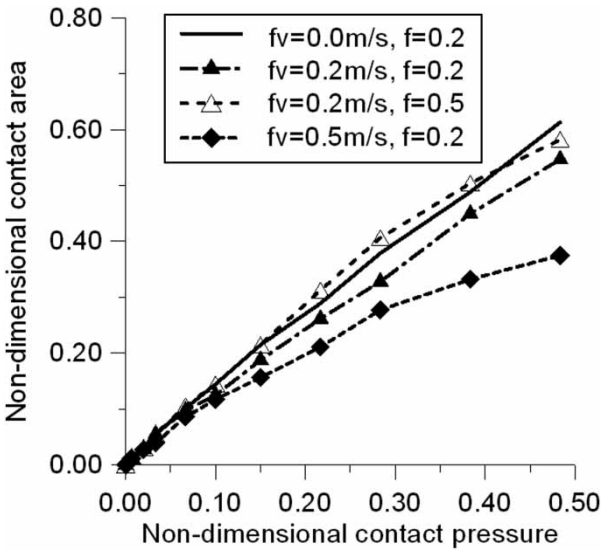

Fig. 11 Relationship between the non-dimensional contact pressure and the non-dimensional contact area under different frictional heat inputs and frictional coefficients when $E_T = 0.1E$

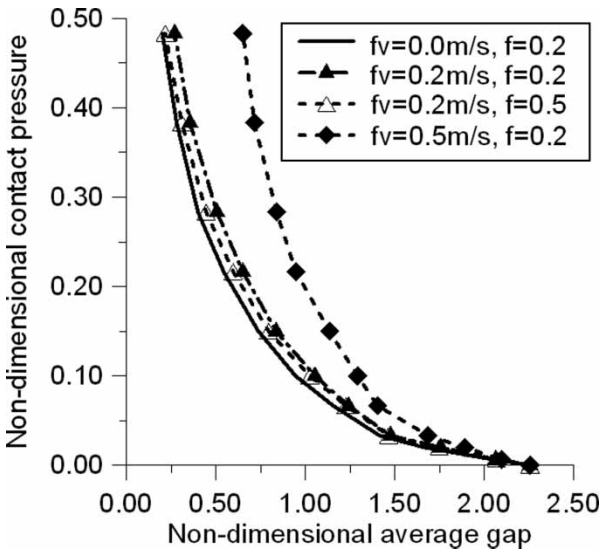

Fig. 12 Relationship between the non-dimensional average gap and the non-dimensional contact pressure under different frictional heat inputs and frictional coefficients when $E_T = 0.1E$

without considering the thermal effect overestimate the real area of contacts, but underestimate the average gap for the contacts between rough surfaces when frictional heating is involved.

6 CONCLUSIONS

A two-dimensional thermal elasto-plastic contact model is developed for analysing of the coupled influence of steady-state frictional heating and elasto-plastic behaviours of the material.

The model is validated by solving a thermal elasto-plastic contact problem between a rigid, isothermal cylinder and a thermal elasto-plastic plane. The thermal elastic, elasto-plastic contact pressure distributions and von Mises stress fields subjected to different frictional heat inputs and frictional coefficients are studied. The results indicate that contact pressures increase with the frictional heat input. The yielding behaviour causes the asymmetry of contact pressure when the effect of the frictional shear is taken into account.

The study of the thermal elasto-plastic contact between a conductive rough surface and a flat, rigid plane shows that when the frictional heat input increases, the maximum contact pressures associated with larger contact areas increase, which indicates that the contacts are more concentrated at larger contact spots. The results suggest that the elasto-plastic models without considering the thermal effect overestimate the real area of contacts, but underestimate the average gap for the contacts between rough surfaces when frictional heating exists.

ACKNOWLEDGEMENTS

The research was supported by the National Natural Science Foundation of China (50475146) and NPU Foundation for Fundamental Research (NPU-FFR-20060500W018101). T. L. would also like to thank the sponsorship of the Alexander von Humboldt Foundation of Germany.

REFERENCES

1 **Ting, B. Y.** and **Winer, W. O.** Friction-induced thermal influences in elastic contact between spherical asperities. *ASME J. Tribol.*, 1989, **111**, 315–322.
2 **Barber, J. R.** Some thermoelastic contact problems involving frictional heating. *Q. J. Mech. Appl. Math.*, 1976, **29**(1), 1–13.
3 **Azarkin, A., Barber, J. R.,** and **Rolf, R. L.** Combined thermal-mechanical effects in frictional sliding. *Key Enging. Materials*, 1989, **33**, 135–160.
4 **Bryant, M. D., Wang, J. P.,** and **Lin, J. W.** Thermal mounding in high speed dry sliders–experiment, theory and comparison. *Wear*, 1995, **181**, 668–677.
5 **Yevtushenko, A. A.** Transient temperature of local moving areas of sliding contact. *Tribol. Int.*, 1997, **30**(3), 209–214.
6 **Ciavarella, M., Decuzzi, P.,** and **Monno, G.** Frictional-excited thermoelastic contact of rough surfaces. *Int. J. Mech. Sci.*, 2000, **42**(7), 1307–1325.
7 **Afferrante, L.** and **Ciavarella, M.** Instability of thermoelastic contact for two half-planes sliding out-of-plane

with contact resistance and frictional heating. *J. Mech. Phy. Solids*, 2004, **52**, 1527–1547.
8 **Wang, Q.** and **Liu, G.** A thermoelastic asperity contact model considering steady-state heat transfer. *STLE Tribol. Trans.*, 1999, **42**, 763–770.
9 **Liu, G.** and **Wang, Q.** Thermoelastic asperity contacts, frictional shear, and parameter correlations. *ASME J. Tribol.*, 2000, **122**, 300–307.
10 **Polonsky, I. A.** and **Keer, L. M.** A fast and accurate method for numerical analysis of elastic layered contacts. *ASME J. Tribol.*, 2000, **122**, 30–35.
11 **Liu, S., Wang, Q. J.,** and **Liu, G.** A versatile method of discrete convolution and FFT (DC-FFT) for contact analyses. *Wear*, 2000, **243**(1–2), 101–111.
12 **Yu, H., Liu, S., Wang, Q. J.,** and **Chung, Y. W.** Influence of temperature-dependent yield strength on thermo-mechanical asperity contacts. *Tribol. Lett.*, 2004, **17**, 155–163.
13 **Boucly, V., Nélias, D., Liu, S., Wang, Q. J.,** and **Keer, L.** Contact analyses for bodies with frictional heating and plastic behavior. *ASME J. Tribol.*, 2005, **127**, 355–364.
14 **Boucly, V., Nélias, D.,** and **Brunet M.** Thermal-elastic-plastic contact analysis for rough bodies with a semi-analytical method. In the ASME/STLE International Joint Tribology Conference, San Diego, CA, USA, 22–24 October 2007.
15 **Liu, G., Zhu, J., Yu, L.,** and **Wang, Q.** Elasto-plastic contact of rough surfaces. *STLE Tribol. Trans.*, 2001, **44**, 437–443.
16 **Argyris, J. H.** and **Scharpf, D. W.** Methods of elasto-plastic analysis. In the Symposium on Finite Element Techniques, Stuttgart, June 1969.
17 **Zienkiewicz, O. Z.** *The finite element method*, 1977 (McGraw-Hill, London).
18 **Johnson K. L.** *Contact mechanics*, 1985 (Cambridge University Press, Cambridge, UK).
19 **Sackfield, A.** and **Hills, D.** A note on the Hertzian contact problem: a correlation of standard formulae. *J. Strain Analysis*, 1983, **18**, 195–197.

APPENDIX

Notation

A	real area of the contact (mm^2)
A_{nom}	nominal contact area (mm^2)
$\mathbf{A}^{\text{m}}$	mechanical influence function matrix
$\mathbf{A}^{\text{t}}$	thermal influence function matrix
ΔA	differential area (mm^2)
$\mathbf{B}$	strain matrix
$\mathbf{D}_{\text{e}}$	elastic matrix
$\mathbf{D}_{\text{p}}$	plastic matrix
$\mathbf{D}_{\text{ep}}$	elasto-plastic matrix
$\boldsymbol{e}$	unit vector
E	Young's modulus (GPa)
E_{T}	elasto-plastic tangential modulus (GPa)
f	frictional coefficient
H'	strain-hardening function (GPa)
$\mathbf{H}$	function that relates equivalent thermal and surface nodal forces
$\mathbf{I}$	identity matrix
J_2'	second deviatoric stress invariant (MPa^2)
k	thermal conductivity (W/m K)
$\mathbf{K}_{\text{e}}$	elastic stiffness matrix
$\mathbf{K}_{\text{p}}$	plastic stiffness matrix
$\mathbf{K}_{\text{ep}}$	elasto-plastic stiffness matrix
n	surface normal
N	number of nodes in the possible region of the surface in contact
$p(x_i)$	contact pressure (MPa)
p^{T}	sum of the pressures of each contact pair on the surface (MPa)
ΔP_j	applied load incremental (N/mm)
$q(x_i)$	frictional heat flux (W/m^2)
$\Delta \boldsymbol{R}^{\text{m}}$	mechanical load increment vector
$\Delta \boldsymbol{R}^{\text{t}}$	thermal load increment vector
$\Delta \boldsymbol{R}_{\sigma}$	initial force vector or unbalanced force vector
$\Delta \mathbf{R}_j^{\text{m}}$	nodal contact force vector of the jth incremental loading
R_i	surface nodal force (N)
R_{ti}	shear loads (N)
R_{ni}	normal loads (N)
T	temperature rise relative to the ambient reference temperature (°C)
T_0	a prescribed ambient reference temperature (°C)
T_{α}^{e}	element average temperature (°C)
$\Delta \boldsymbol{u}$	displacement vector
$\Delta \boldsymbol{u}_{\text{I}}$	plastic deformation vector
$\Delta \boldsymbol{u}_{\text{e}}^{\text{m}}$	elastic mechanical deformation vector
$\Delta \boldsymbol{u}_{\text{e}}^{\text{t}}$	thermoelastic deformation vector
v	sliding speed (m/s)
x_i	surface nodal coordinates along x-axis (mm)
$\boldsymbol{y}_0$	surface original separation vector
$\boldsymbol{y}_j$	surface separation vector or slack vector at the jth incremental loading
$\Delta \alpha_j$	rigid-body displacement increment at the jth incremental loading (mm)
β	heat partition coefficient
$\boldsymbol{\varepsilon}$	strain vector
$\boldsymbol{\varepsilon}_0$	free thermal strain vector
$\Delta \boldsymbol{\varepsilon}$	incremental strain vector
$\Delta \boldsymbol{\varepsilon}_0$	incremental free thermal strain vector
θ	thermal expansion coefficient (μm/mK)
ν	Poisson's ratio
$\Delta \boldsymbol{\sigma}$	stress increment vector
$\Delta \boldsymbol{\sigma}_0$	incremental initial stress vector
σ_{e}	equivalent von Mises stress (MPa)
σ_{vm}	maximum von Mises stress (MPa)
σ_{Y}	yield strength of the material (MPa)
$\bar{\sigma}$	average stress (MPa)
Ω	solid domain